Research Article | Vol. 24, No. 15 | 25 Jul 2016 | OPTICS EXPRESS 16788

Optics EXPRESS

Low chromatic Fresnel lens for broadband attosecond XUV pulse applications

HUAIHAI PAN,[1,2,3] CHRISTIAN SPÄTH,[2,3] ALEXANDER GUGGENMOS,[2,3] SOO HOON CHEW,[2,3] JÜRGEN SCHMIDT,[2,3] QUAN-ZHONG ZHAO,[1] AND ULF KLEINEBERG,[2,3,*]

[1]*State Key Laboratory of High Field Laser Physics, Shanghai Institute of Optics and Fine Mechanics, Chinese Academy of Sciences, Shanghai 201800, China*
[2]*Max-Planck-Institut für Quantenoptik, Hans-Kopfermann-Str. 1,85748 Garching, Germany*
[3]*Ludwig-Maximilians-Universität München, Fakultät für Physik, Am Coulombwall 1, 85748 Garching, Germany*
[*]*ulf.kleineberg@physik.uni-muenchen.de*

Abstract: Fresnel zone plates show a great potential in achieving high spatial resolution imaging or focusing for XUV and soft/hard X-ray radiation, however they are usually strictly monochromatic due to strong chromatic dispersion and thus do not support broad radiation spectra, preventing their application to attosecond XUV pulses. Here we report on the design and theoretical simulations based on the design of an achromatic hybrid optics combining both, a refractive and diffractive lens in one optical element. We are able to show by calculation that the chromatic dispersion along the optical axis can be greatly reduced compared to a standard Fresnel zone plate while preserving the temporal structure of the attosecond XUV pulses at focus.

OCIS codes: (050.1965) Diffractive lenses; (180.5810) Scanning microscopy; (040.6040) Silicon; (180.7460) X-ray microscopy; (230.3990) Micro-optical devices;

References and links

1. S. Driever, K. B. Holzner, J.-C. Delagnes, N. Fedorov, M. Arnold, D. Bigourd, F. Burgy, D. Descamps, E. Cormier, R. Guichard, E. Constant, and A. Zaïr, "Near infrared few-cycle pulses for high harmonic generation," J. Phys. At. Mol. Opt. Phys. **47**(20), 204013 (2014).
2. G. Vampa, C. R. McDonald, G. Orlando, D. D. Klug, P. B. Corkum, and T. Brabec, "Theoretical analysis of high-harmonic generation in solids," Phys. Rev. Lett. **113**(7), 073901 (2014).
3. N. Ishii, K. Kaneshima, K. Kitano, T. Kanai, S. Watanabe, and J. Itatani, "Carrier-envelope phase-dependent high harmonic generation in the water window using few-cycle infrared pulses," Nat. Commun. **5**, 3331 (2014).
4. M. Drescher, M. Hentschel, R. Kienberger, G. Tempea, C. Spielmann, G. A. Reider, P. B. Corkum, and F. Krausz, "X-ray pulses approaching the attosecond frontier," Science **291**(5510), 1923–1927 (2001).
5. S. P. Hau-Riege and H. N. Chapman, "Reflection of attosecond x-ray free electron laser pulses," Rev. Sci. Instrum. **78**(1), 013104 (2007).
6. L. Poletto, F. Frassetto, F. Calegari, S. Anumula, A. Trabattoni, and M. Nisoli, "Micro-focusing of attosecond pulses by grazing-incidence toroidal mirrors," Opt. Express **21**(11), 13040–13051 (2013).
7. H. Motoyama, T. Sato, A. Iwasaki, Y. Takei, T. Kume, S. Egawa, K. Hiraguri, H. Hashizume, K. Yamanouchi, and H. Mimura, "Development of high-order harmonic focusing system based on ellipsoidal mirror," Rev. Sci. Instrum. **87**(5), 051803 (2016).
8. M. Hofstetter, A. Aquila, M. Schultze, A. Guggenmos, S. Yang, E. Gullikson, M. Huth, B. Nickel, J. Gagnon, V. S. Yakovlev, E. Goulielmakis, F. Krausz, and U. Kleineberg, "Lanthanum-molybdenum multilayer mirrors for attosecond pulses between 80 and 130 eV," New J. Phys. **13**(6), 063038 (2011).
9. A. Guggenmos, M. Jobst, M. Ossiander, S. Radünz, J. Riemensberger, M. Schäffer, A. Akil, C. Jakubeit, P. Böhm, S. Noever, B. Nickel, R. Kienberger, and U. Kleineberg, "Chromium/scandium multilayer mirrors for isolated attosecond pulses at 145 eV," Opt. Lett. **40**(12), 2846–2849 (2015).
10. W. Chao, B. D. Harteneck, J. A. Liddle, E. H. Anderson, and D. T. Attwood, "Soft X-ray microscopy at a spatial resolution better than 15 nm," Nature **435**(7046), 1210–1213 (2005).
11. A. Sakdinawat and D. Attwood, "Nanoscale X-ray imaging," Nat. Photonics **4**(12), 840–848 (2010).
12. C. David, S. Gorelick, S. Rutishauser, J. Krzywinski, J. Vila-Comamala, V. A. Guzenko, O. Bunk, E. Färm, M. Ritala, M. Cammarata, D. M. Fritz, R. Barrett, L. Samoylova, J. Grünert, and H. Sinn, "Nanofocusing of hard X-ray free electron laser pulses using diamond based Fresnel zone plates," Sci. Rep. **1**, 57 (2011).

#262901 http://dx.doi.org/10.1364/OE.24.016788
Journal © 2016 Received 11 Apr 2016; revised 29 Jun 2016; accepted 29 Jun 2016; published 15 Jul 2016

Optics EXPRESS

13. R. Kienberger, E. Goulielmakis, M. Uiberacker, A. Baltuska, V. Yakovlev, F. Bammer, A. Scrinzi, T. Westerwalbesloh, U. Kleineberg, U. Heinzmann, M. Drescher, and F. Krausz, "Atomic transient recorder," Nature **427**(6977), 817–821 (2004).
14. M. Hentschel, R. Kienberger, C. Spielmann, G. A. Reider, N. Milosevic, T. Brabec, P. Corkum, U. Heinzmann, M. Drescher, and F. Krausz, "Attosecond metrology," Nature **414**(6863), 509–513 (2001).
15. M. Drescher, M. Hentschel, R. Kienberger, M. Uiberacker, V. Yakovlev, A. Scrinzi, T. Westerwalbesloh, U. Kleineberg, U. Heinzmann, and F. Krausz, "Time-resolved atomic inner-shell spectroscopy," Nature **419**(6909), 803–807 (2002).
16. T. Sekikawa, A. Kosuge, T. Kanai, and S. Watanabe, "Nonlinear optics in the extreme ultraviolet," Nature **432**(7017), 605–608 (2004).
17. S. Watanabe, "Attosecond pulse characterization by XUV nonlinear optics," in *Conference on Lasers and Electro-Optics/Quantum Electronics and Laser Science Conference and Photonic Applications Systems Technologies*, Technical Digest (CD) (Optical Society of America, 2006), paper CFF3.
18. L. Young, E. P. Kanter, B. Krässig, Y. Li, A. M. March, S. T. Pratt, R. Santra, S. H. Southworth, N. Rohringer, L. F. Dimauro, G. Doumy, C. A. Roedig, N. Berrah, L. Fang, M. Hoener, P. H. Bucksbaum, J. P. Cryan, S. Ghimire, J. M. Glownia, D. A. Reis, J. D. Bozek, C. Bostedt, and M. Messerschmidt, "Femtosecond electronic response of atoms to ultra-intense X-rays," Nature **466**(7302), 56–61 (2010).
19. R. Kienberger, M. Hentschel, M. Uiberacker, Ch. Spielmann, M. Kitzler, A. Scrinzi, M. Wieland, T. Westerwalbesloh, U. Kleineberg, U. Heinzmann, M. Drescher, and F. Krausz, "Steering attosecond electron wave packets with light," Science **297**(5584), 1144–1148 (2002).
20. D. Attwood, *Soft X-Rays and Extreme Ultraviolet Radiation: Principles and Applications* (Cambridge University Press, 1999).
21. W. Chao, J. Kim, S. Rekawa, P. Fischer, and E. H. Anderson, "Demonstration of 12 nm Resolution Fresnel Zone Plate Lens based Soft X-ray Microscopy," Opt. Express **17**(20), 17669–17677 (2009).
22. K. Jefimovs, J. Vila-Comamala, T. Pilvi, J. Raabe, M. Ritala, and C. David, "Zone-doubling technique to produce ultrahigh-resolution x-ray optics," Phys. Rev. Lett. **99**(26), 264801 (2007).
23. M. Wieland, Ch. Spielmann, U. Kleineberg, T. Westerwalbesloh, U. Heinzmann, and T. Wilhein, "Toward time-resolved soft X-ray microscopy using pulsed fs-high-harmonic radiation," Ultramicroscopy **102**(2), 93–100 (2005).
24. R. Ashman and M. Gu, "Effect of ultrashort pulsed illumination on foci caused by a Fresnel zone plate," Appl. Opt. **42**(10), 1852–1855 (2003).
25. Y. Wang, W. Yun, and C. Jacobsen, "Achromatic Fresnel optics for wideband extreme-ultraviolet and X-ray imaging," Nature **424**(6944), 50–53 (2003).
26. E. Goulielmakis, M. Uiberacker, R. Kienberger, A. Baltuska, V. Yakovlev, A. Scrinzi, T. Westerwalbesloh, U. Kleineberg, U. Heinzmann, M. Drescher, and F. Krausz, "Direct measurement of light waves," Science **305**(5688), 1267–1269 (2004).
27. V. A. Antonov, Y. V. Radeonychev, and O. Kocharovskaya, "Formation of a single attosecond pulse via interaction of resonant radiation with a strongly perturbed atomic transition," Phys. Rev. Lett. **110**(21), 213903 (2013).
28. V. A. Polovinkin, Y. V. Radeonychev, and O. Kocharovskaya, "Few-cycle attosecond pulses via periodic resonance interaction with hydrogenlike atoms," Opt. Lett. **36**(12), 2296–2298 (2011).
29. P. Anderson, P. Horak, J. G. Frey, and W. S. Brocklesby, "Isolated attosecond pulses by self-compression in short gas-filled fibers," in *Lasers and Electro-Optics Europe (CLEO EUROPE/IQEC), 2013 Conference on and International Quantum Electronics Conference* (IEEE, 2013), 1.
30. B. L. Henke, E. M. Gullikson, and J. C. Davis, "X-Ray interactions: photoabsorption, scattering, transmission, and reflection at E = 50-30,000 eV, Z = 1-92," At. Data Nucl. Data Tables **54**(2), 181–342 (1993).
31. J. Kirz, "Phase zone plates for x rays and the extreme uv," J. Opt. Soc. Am. **64**(3), 301–309 (1974).
32. A. Sakdinawat and Y. Liu, "Phase contrast soft x-ray microscopy using Zernike zone plates," Opt. Express **16**(3), 1559–1564 (2008).
33. E. Di Fabrizio, F. Romanato, M. Gentili, S. Cabrini, B. Kaulich, J. Susini, and R. Barrett, "High-efficiency multilevel zone plates for keV X-rays," Nature **401**(6756), 895–898 (1999).

1. Introduction

High harmonic generation (HHG) from the interaction of intense few-cycle femtosecond laser pulses with a gaseous or solid target [1–3], which can produce attosecond pulses at short wavelength [4], requires the fabrication and utilization of extreme ultraviolet (XUV) and soft X-ray optics for spectral filtering, temporal shaping and steering such pulses onto the target under investigation. While in current attosecond experiments typically grazing incidence reflectors [5, 6], ellipsoidal mirror for focusing HHG radiation [7], or normal incidence multilayer mirrors [8, 9] with microscopic spot sizes are used, the application of attosecond spectroscopy to nano-scaled targets requires new types of optics, that are capable of achieving nanoscopic spatial resolution comparable to applications in XUV and soft X-ray microscopes

Optics EXPRESS

[10–12]. These XUV and soft X-ray optics could possibly be utilized in attosecond time-resolved pump-probe experiments to observe the fast electronic dynamics of atoms or molecules in nanoscale systems [13–15]. Furthermore, the increase in focused XUV pulse intensity opens the potential for non-linear XUV experiments [16, 17]. For instance, the multicore-shell ionization or recombination of atoms [18] could be studied with a pump-probe technique [19] in which two attosecond pulses are used, the first attosecond pulse as pump to excite the core-shell of atoms and the second attosecond pulse as probe to measure the pump-induced changes. However, the spectrum of attosecond pulses generated from HHG is in the wavelength range of the XUV (i.e., from 30 eV to 250 eV) and soft X-ray (i.e., from 250 eV to several keV) [20], which makes conventional refractive optics inappropriate for focusing such attosecond pulses due to high absorption and low capability of light bending upon XUV illumination. Reflective nanofocusing optics typically suffers from strong image aberrations (astigmatism or spherical aberrations) and/or low numerical aperture (NA). In contrary, Fresnel zone plates (FZP) as circular diffractive optics are capable of focusing XUV and soft X-ray radiation to a nanospot by diffraction rather than refraction with high NA and vanishing spherical aberration in the focal plane, and therefore overcome the aforementioned disadvantages in conventional refractive or reflective optics [10, 21, 22]. Until now, using FZP to focus femtosecond HHG radiation has been reported, which realizes a very high spatial resolution of 200 nm, as well as high temporal resolution up to femtosecond scale [23]. However, to achieve such a high spatial resolution focusing with a FZP, a highly monochromatic XUV or soft X-ray beam at the input is required. Consequently, broad bandwidth sources such as XUV or soft X-ray radiation from HHG will pose an issue when utilizing such optics. The strong chromatic dispersion produced by a FZP from such broad wavelength sources does not only result in image blurring along the optical axis (i.e., z-axis) [24] but also broadens the duration of attosecond pulses at the first order focus, thus destroying the temporal structure of attosecond pulses. In order to decrease the chromatic dispersion of a conventional FZP when applied to broadband XUV or soft X-ray sources, a new type of optics design was proposed by Chris Jacobsen et al. [25], who suggested to employ an additional refractive lens with positive chromatic dispersion to compensate for the intrinsic negative chromatic dispersion produced by the FZP.

Here we report on extended theoretical simulations of the spatiotemporal focusing properties of such achromatic optics, as a combination of a FZP and a conventional refractive lens, when being applied to a broadband attosecond soft x-ray pulse from HHG. We have investigated the key parameters such as spatial intensity distribution and temporal intensity distribution of an attosecond XUV pulse diffracted by achromatic optics at the optical axis (e.g., at first order focus). The impinging attosecond XUV pulse employed here for simulations is centered at 92 eV with a duration of 120 as, as it is typical for many attosecond experiments [26–29]. Silicon (Si) was used as a refractive lens material in the simulations since it has a very high positive dispersion around 92 eV for compensating the negative dispersion given by FZP. Molybdenum (Mo) was selected as the material for FZP, phase-reverse zone plate (RZP) and multilevel zone plate (MZP) because of its low absorption at 92 eV. Finally, silicon nitride was utilized as a substrate for its better optical transparent property. The theoretical simulation results show that we are able to achieve a higher spatial resolution as well as preserve the temporal structure of the attosecond XUV pulse at the first diffraction order using this achromatic optics design. Our achromatic optics design concept and theoretical results provide great application potential such as time-resolved photoemission XUV microscopy for observing the dynamics of electrons in inner-shell core of atoms at the nanoscale using this pump-probe technique.

2. Design of the optical device

The first order focal length of an FZP has an inverse relationship to the wavelength, which can be described as follows:

Optics EXPRESS

$$f = \frac{4N(\Delta r)^2}{\lambda}. \tag{1}$$

where f is the focal length, N is the total number of zones, Δr is the outermost zone width and λ is the wavelength. This strong inverse relationship between focal length and wavelength results in a high chromatic dispersion. Here, the optical devices (e.g., FZP) of inverse correlation between f_z and λ, are called negative chromatic optics, others are called positive chromatic optics. To compensate the large negative chromatic dispersion of a FZP, a refractive lens with positive chromatic dispersion can be applied. For a thin refractive lens with a single-curved surface (plano-convex), the focal length can be written as follows:

$$f_R = \frac{R_C}{n-1}. \tag{2}$$

where f_R is the focal length, R_C is the curvature radius, n is the refractive index. When the radiation is in the XUV and soft X-ray wavelength range, the refractive index is given by:

$$n = 1-\delta+i\beta = 1-\alpha\lambda^2 f_1 + i\alpha\lambda^2 f_2 = 1-\frac{n_a r_e}{2\pi}\lambda^2(f_1 - if_2). \tag{3}$$

where |α|&|β|<<1 [20], n_a is the electron density per unit volume, r_e is the classical electron radius, λ is the wavelength and $f_1 - if_2$ is the complex atomic scattering factor. Ignoring the imaginary part of the refractive index (no absorption), the focal length of the lens can be rewritten as follows:

$$f_R = \frac{R_C}{-\delta} = \frac{R_C}{-\alpha\lambda^2 f_1}. \tag{4}$$

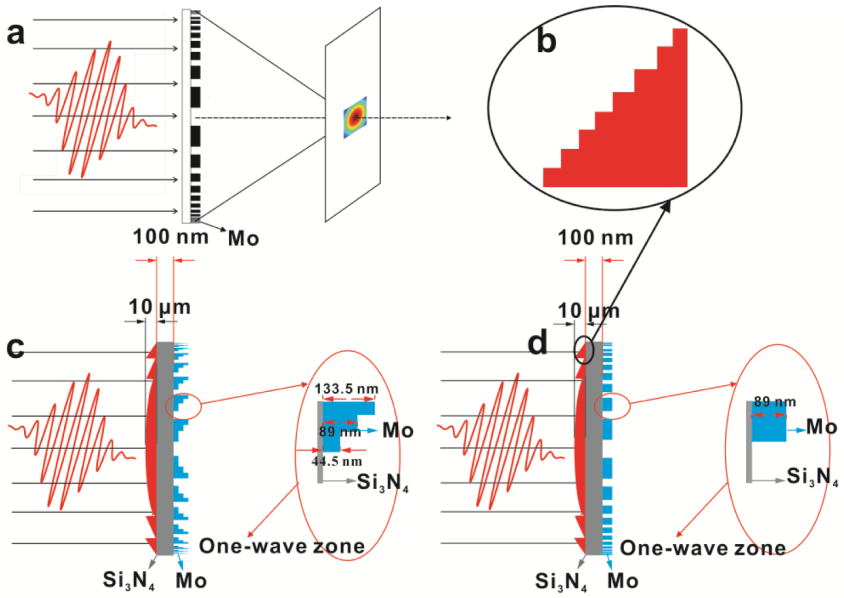

Fig. 1. A sketch of the achromatic diffractive-refractive hybrid XUV optics. (a) Ideal zone plate with totally transparent zone rings and totally opaque zone rings. (b)The principle of fabrication of micro-lens. (c) Achromatic optical device combined with multilevel zone plate. (d) Achromatic optical device combined with phase-reverse zone plate.

Optics EXPRESS

Figure 1 shows the schematic representation of our optical device design (so-called achromatic optical device (AOD)), in which the refractive lens is fabricated on one side of a 100 nm thick Si_3Ni_4 membrane and the multilevel zone plate (MZP) or phase-reverse zone plate (RZP) is fabricated on the other side. The sketch of ideal FZP with totally transparent zone rings and totally opaque zone rings is given in Fig. 1(a). Meanwhile, Figs. 1(c) and 1(d) also give the sketchs of AOD with MZP, or RZP, respectively. These AOD with MZP or RZP, can be fabricated step by step as shown in Fig. 1(b), which will be able to keep the single curvature of lens via increasing the steps of fabrication, but also increase the difficulties of fabrication due to the accuracy for calabration of every step. However, the detailed process of fabrication will not been discussed in present work. For the AOD as shown in Figs. 1(c) and 1(d), the equivalent focal length can be written as follows:

$$\frac{1}{f}=\frac{1}{f_z}+\frac{1}{f_R}=\frac{\lambda}{4N(\Delta r)^2}-\frac{\alpha\lambda^2 f_1}{R_C}. \tag{5}$$

where f is the equivalent focal length of the AOD. If the derivative of the equivalent focal length f with respect to the wavelength λ becomes zero for a specific refractive material in the XUV or soft X-ray wavelength range, this new optical device will become fully achromatic. Assuming this derivative is zero, we will then obtain the following mathematical relation:

$$\frac{f_R}{f_z}=-(2+D). \tag{6}$$

where $D\equiv(\partial f_1/\partial\lambda)\cdot(\lambda/f_1)$ characterizes the dispersion of the refractive material. Based on Eqs. (2) and (6), if assuming the dipersion D is a constant, the curvature radius of the refractive lens could be written as follows:

$$R_C\approx(2+D)\alpha\lambda^2 f_1 f_z=(2+D)\delta f_z. \tag{7}$$

The dispersion D tends to be a large positive value near absorption edges in the XUV or soft X-ray spectral range, as shown in Fig. 2.

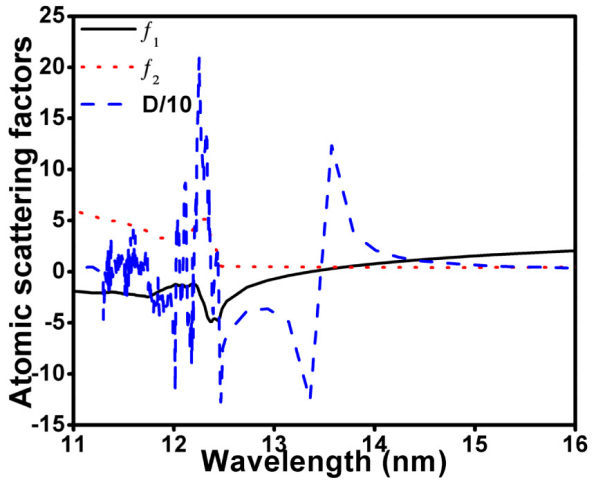

Fig. 2. The atomic scattering factor of Si are plotted against wavelength, three color lines represent f_1, f_2, and dispersion defined by D, respectively. (Data from the Center for X-Ray Optics [30]).

Optics EXPRESS

The dispersion D of Si is approximately 100 around the wavelength of 13.5 nm. Therefore, it is appropriate to use Si as the material for fabricating the refractive lens to compensate the high negative chromatic dispersion produced by the FZP with XUV illumination around 13.5 nm. The curvature radius of the refractive lens can be estimated as 100 μm if the focal length of the FZP is set to 1 mm and dispersion of material is assumed to be 100. However, due to the imaginary part of the refractive index of Si (see Fig. 2), it will produce absorption when the XUV or soft X-ray photons penetrate the refractive lens made out of Si, thus decreasing the diffractive efficiency of AOD. The Fresnel refractive lens with a single-surface curvature with a maximum thickness of 10 μm can be used to replace the conventional refractive lens, as shown in Fig. 1. The Fresnel refractive lens consists of concentric annulus with same curvature and same thickness. When light passes from a medium (i.e. air) to another medium (i.e. Fresnel refractive lens), the bending of light is only dependent on the refractive index and the interface between air and lens, the lens thickness has no effect on the bending of light, thus the Fresnel refractive lens has almost the same capability of bending light to a focus compared to a conventional refractive lens with more total thickness, finally reducing the absorption in a Fresnel refractive lens compared to a conventional refractive lens. Another approach taken is to replace the conventional FZP by a RZP (See Fig. 1(c)) [31, 32] or MZP (i.e., four-level zone plate) [33], as shown in Fig. 2(b), as alternative for future technoglogy, which are able to improve the diffractive efficiency greatly compared to the FZP. The element Mo was chosen for the design of the RZP and MZP. For the RZP, the thickness of every non-transparent zone was set to 89.5 nm, as shown in Fig. 1(c). And for the MZP, the thickness of non-transparent zone for each one-wave zone was designed to be 44.5 nm, 89 nm and 135.5 nm, respectively, as shown in Fig. 1(b).

Using the AOD (see Figs. 1(b) and 1(c)), the attosecond XUV pulses can be focused to a small spatial spot both on the optical axis (z-axis) and in the focal plane, thus preserving the temporal structure of an attosecond pulse. It has been known that the diffractive pattern of monochromatic light produced by a circular aperture can be calculated using the Fresnel-Kirchhoff diffraction formula. In contrast to monochromatic radiation, attosecond XUV pulses centered at 92 eV with durations of 120 as and 500 as consist of a broad bandwidth spectrum. Here we define the full width at half maximum (FWHM) of a Gaussian pulse as pulse duration and FWHM of corresponding spectra as bandwidth. Therefore, for the 120 as pulse, it has 15.2 eV bandwidth, and for the 500 as pulse, it has 3.65 eV bandwidth, as shown in Figs. 3(c) and 3(d).

Optics EXPRESS

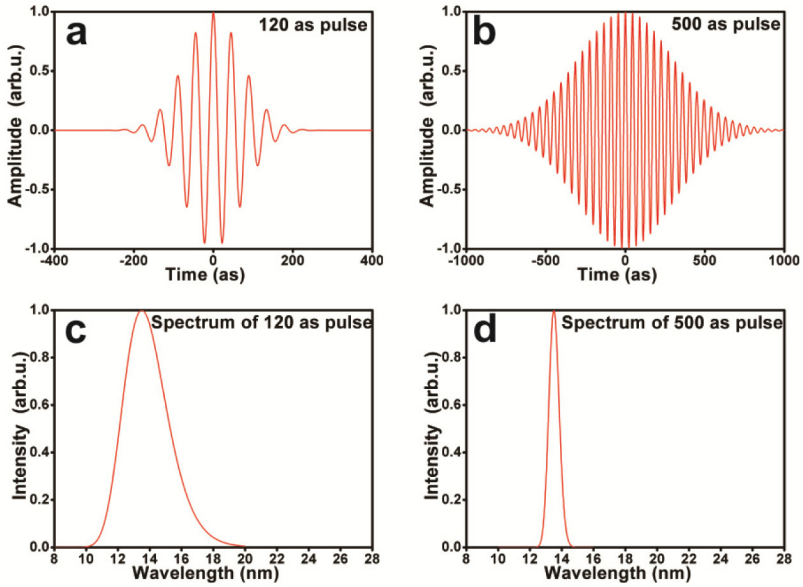

Fig. 3. (a) Electric field of an attosecond pulse with a duration of 120 as is plotted against time. (b) Electric field of an attosecond pulse with a duration of 500 as is plotted against time. (c) The corresponding spectrum of the pulse in Fig. 3(a). (d) The corresponding spectrum of the pulse in Fig. 3(b).

When using these pulses to illuminate the FZP and AOD (see Figs. 1), the pulses can be seen as a composition of continuous spectrum with a certain initial phase. The corresponding Fourier transformation to the frequency domain is given by the following formula:

$$E(r,\theta,w)=\frac{1}{2\pi}\int_0^{\infty}E(r,t)e^{-i\omega t}dt. \tag{8}$$

Therefore, using the reverse Fourier transformation, the time-averaged intensity of attosecond XUV pulses focused by the FZP can be calculated via the following formula:

$$I_{out}(x,y,z)=\int_0^{\infty}\left|\frac{1}{i\lambda}\sum_{j=1}^{J}\int_{R_j}^{R_{j+1/2}}\int_0^{2\pi}\eta e^{i\phi}E(r,\theta,\omega)\frac{e^{i(2\pi/\lambda)R}}{R}drd\theta\right|^2 d\omega. \tag{9}$$

where λ is the wavelength, R_j and $R_{j+1/2}$ are the radius of zone r_j and $r_{j+1/2}$ that can be written in the form of $R_j=\sqrt{2(j-1)f\lambda}$ and $R_{j+1/2}=\sqrt{2(j-1/2)f\lambda}$, R is the distance between source point (r,θ) on the zone plate and observation point (x,y,z), which can be described as the following formula:

$$R=\sqrt{z^2+(r\cos\theta-x)^2+(r\sin\theta-y)^2}. \tag{10}$$

and ϕ consists of a phase term and an absorption term produced by the lens and can be written as $\phi=i\cdot(2\pi/\lambda)\cdot n\cdot d$, in which d represents the thickness and n the refractive index of the lens, as shown in Eq. (3) and Fig. 1. η represents the amplitude coefficient.

Optics EXPRESS

Besides the time-averaged intensity of attosecond XUV pulse at focus of FZP and AOD, the temporal structure at focus is also important, which can be calculated as the following formula:

$$I_{out}(x,y,z,t)=\left|\int_0^{\infty}e^{-i\omega t}\frac{1}{i\lambda}\sum_{j=1}^{J}\int_{R_j}^{R_{j+1/2}}\int_0^{2\pi}\eta e^{i\phi}E(r,\theta,\omega)\frac{e^{i(2\pi/\lambda)R}}{R}drd\theta d\omega\right|^2 \qquad (11)$$

where t is the time of light propagation between the source point on the AOD and the fixed point in the image coordinate system. Using this equation, we can obtain the temporal intensity distribution of an attosecond XUV pulse at the first order focus of our AOD.

3. Simulation and discussion

The oscillating electric field of attosecond XUV pulses centered at a wavelength of 13.5 nm with two different durations of 120 as and 500 as are shown in Figs. 3(a) and 3(b), respectively, whose peak amplitudes are normalized to 1 and the corresponding spectra are shown in Figs. 3(c) and 3(d), respectively. The XUV pulse is supposed to have a plane wave with a Gaussian frequency distribution and have the normalized spatial coherence degree of 1, and the pulses employed in our paper are Fourier-limited pulses. As shown in Figs. 3(c) and 3(d), a pulse with a duration of 120 attoseconds as shown in Fig. 3(a) has a broader bandwidth compared to the pulse with a duration of 500 attoseconds as shown in Fig. 3(b), which implies a shorter pulse duration in the time domain but more spectral components in the corresponding frequency domain. Next, three different designs of optical devices will be discussed. First the conventional FZP that consists of 120 transparent half-wave zones (whose radius is 56.8 μm and outermost width is 118 nm), as shown in Fig. 1(a), second the AOD consisting of MZP with 120 one-wave zones (see Fig. 1(c)) and third the AOD consisting of RZP with 120 half-wave zones (see Fig. 1(d)). Figure 4(a) shows the time-averaged intensity distribution of an attosecond XUV pulse with a duration of 120 as by the FZP and other two different kinds of AODs along the optical axis (i.e., z-axis), using Eq. (9). For the case of 120 as XUV pulse illumination, as illustrated in Fig. 4(a), the FZP produces a strong chromatic dispersion along the optical axis in the image coordinate system, which can degrade the image quality. In contrast to the FZP, the AODs of either MZP or RZP (see Figs. 1(c) and 1(d)) can greatly decrease the chromatic dispersion along the optical axis in the image coordinate system. On the other hand, there is not much difference in chromatic dispersion for these three optical devices in the case of 500 as XUV pulse illumination, as shown in Fig. 4(b). It is obvious that the chromatic dispersion for all three devices is less in the case of 500 as XUV pulse illumination than that of 120 as, since 500 as XUV pulses have a narrower bandwidth. From Fig. 4(a), we can also observe that compared to the AOD consisting of RZP, the AOD consisting of MZP can improve the time-averaged intensity while suppressing the other higher order diffractions (i.e. third order diffraction at 0.3 mm). In comparison to the FZP design, both AODs have slightly shifted its focus from 1.0 mm to 1.003 mm (not shown in Fig. 4(a)) due to the refractive effect of the lens, which can be obtained from Eq. (5). Meanwhile, the focus of AODs in the case of 500 as XUV pulse illumination is shifted to 1.01 mm (not shown in Fig. 4(b). The different positions of the focus between the cases of Figs. 4(a) and 4(b) can be explained by the different spectral components of XUV pulses because of different pulse durations.

Optics EXPRESS

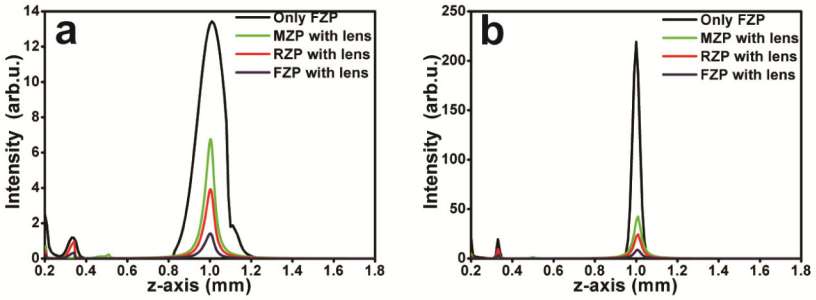

Fig. 4. The time-averaged intensity distribution along the optical axis of FZP, MZP with lens, and RZP with lens, respectively (a) in the case of illumination of 120 as XUV pulse, (b) in the case of illumination of 500 XUV pulse.

Figures 5(a) and 5(b) present the corresponding time-averaged intensity off-axis of Figs. 4(a) and 4(b) at the focus (i.e., R-axis on the focal plane) using Eq. (9). Here, the full width at half maximum (FWHM) of the focused light intensity profile on the focal plane was utilized to define the spatial resolution of these optical devices under illumination of pulses with different durations. In case of the 120 as pulse, as shown in Fig. 5(a), the FZP has a spatial resolution of 126 nm and both AODs of either MZP or RZP have a spatial resolution of 116 nm. Therefore, it implies that AODs can obtain a higher spatial resolution compared to the FZP. Similarly, for the case of a 500 as pulse, the FZP has a spatial resolution of 126 nm and both AODs have the same spatial resolution of 118 nm on the focal plane, as shown in Fig. 5(b). Comparing Figs. 5(a) and 5(b), we can conclude that the pulse duration hardly has an influence on the spatial resolution. Furthermore, we also find that longer a pulse duration can achieve much higher time-averaged intensity for the optical devices.

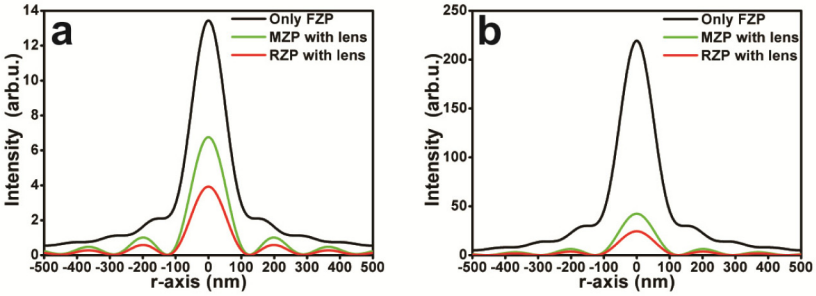

Fig. 5. The time-averaged intensity distribution off-axis of FZP, MZP with lens, and RZP with lens, respectively, (a) in the case of illumination of 120 as XUV pulse, (b) in the case of illumination of 500 as XUV pulse.

Besides the time-averaged intensity on and off-axis of diffractive patterns as shown in Figs. 4 and 5, the temporal structure of a focused XUV pulse at the focus of these optical devices is also a very important parameter to be studied. Using Eq. (11), the temporal intensity distribution of a focused XUV pulse against time at the focus for these three optical devices under the illumination of pulses with durations of 120 and 500 as was obtained, as shown in Figs. 6(a) and 6(d), respectively. Here, we also used the FWHM of the focused XUV intensity profile versus time to define the temporal structure of the XUV pulse at focus (i.e., the duration of the focused XUV pulse at focus). Figure 6(a) shows that a pulse with 5.25 fs at focus is produced upon the 120 as illumination on the FZP. In contrast, AODs of either MZP or RZP produces a pulse of only 230 as at focus for the case of the 120 as pulse,

Optics EXPRESS

in which the temporal structure of the incident XUV pulse is almost preserved. It is also shown that AOD of MZP could obtain a higher peak intensity than AOD of RZP. For the case of the 500 as pulse in Fig. 6(b), it shows the similar results as in Fig. 6(a). A pulse with a duration of 5.17 fs at focus is produced when employing FZP, and a shorter pulse duration of 535 as is obtained using both AODs of MZP and RZP, respectively. It is the same case here that the 500 as pulse could achieve a much higher peak intensity at focus compared to the 120 as pulse. According to the Huygens-Frensel principle, when a single attosecond XUV pulse illuminates the FZP, the subpulses from different transparent zones propagate to the focus and constructively interfere. Due to the optical path difference (OPD) between different transparent zones and focus, it will produce a time delay at focus among subpulses from different transparent zones, consequently producing a longer pulse with a lower peak intensity. However, as shown in Fig. 1, when employing both AODs of either MZP or RZP, OPD at focus among subpulses from different zones can be compensated via the lens, thus, compressing the pulse duration and improving its peak intensity compared to the case of FZP.

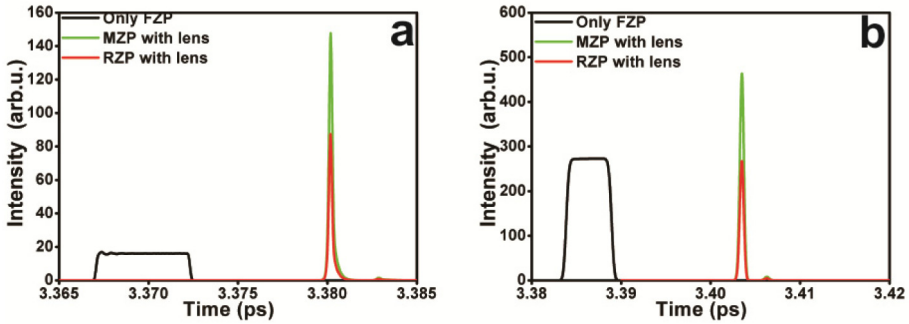

Fig. 6. The temporal intensity distribution at focus of FZP, MZP with lens, and RZP with lens, respectively, (a) in the case of illumination of 120 as XUV pulse, (b) in the case of illumination of 500 as XUV pulse.

It is well known that the spatial resolution of a FZP is dependent on the outermost zone width. Therefore, the more zones of a FZP we fabricate, the higher spatial resolution of a FZP we can obtain. For the AODs, the spatial resolution is also dependent on the outermost zone width of MZP or RZP on the one side of AODs. In order to get a higher spatial resolution as well as to preserve an ultrashort XUV pulse at focus of the AOD, the temporal structure of the focused XUV pulse at focus of the AOD was investigated for different zone numbers. Figures 7(a)–7(d) show the temporal intensity distribution of the focused XUV pulse at focus upon 120 as pulse illumination on AODs of MZP with different zone numbers. When the zone number is 50, as shown in Fig. 7(a), the peak intensity of the focused XUV is approximately 0.4 that is smaller than the peak intensity of the incident XUV pulse (peak intensity of incident XUV pulse is 1). Increasing the zone number from 50 to 130, as shown in Figs. 7(b)-7(d), the peak intensity of the focused XUV pulse increases from 0.4 to 140. When the zone number is increased to 100, the peak intensity reaches a plateau (i.e., 140), which can be attributed to the high average absorption of the lens when an XUV pulse passes through the lens. The larger the zone number of the AOD, the bigger is the diameter of the AOD, and the larger is the corresponding average thickness of the lens, thus, producing the high average absorption of the lens when an XUV pulse passes through it. Compared to Figs. 7(c) and 7(d) show that varying the zone number from 100 to 130 hardly increases the peak intensity, but can produce double pulses at focus, where the time delay between two pulses is about 3 fs. Therefore, to get a higher spatial resolution and preserve a single pulse with short duration at focus, the AOD of MZP with 120 zones is the appropriate option.

Optics EXPRESS

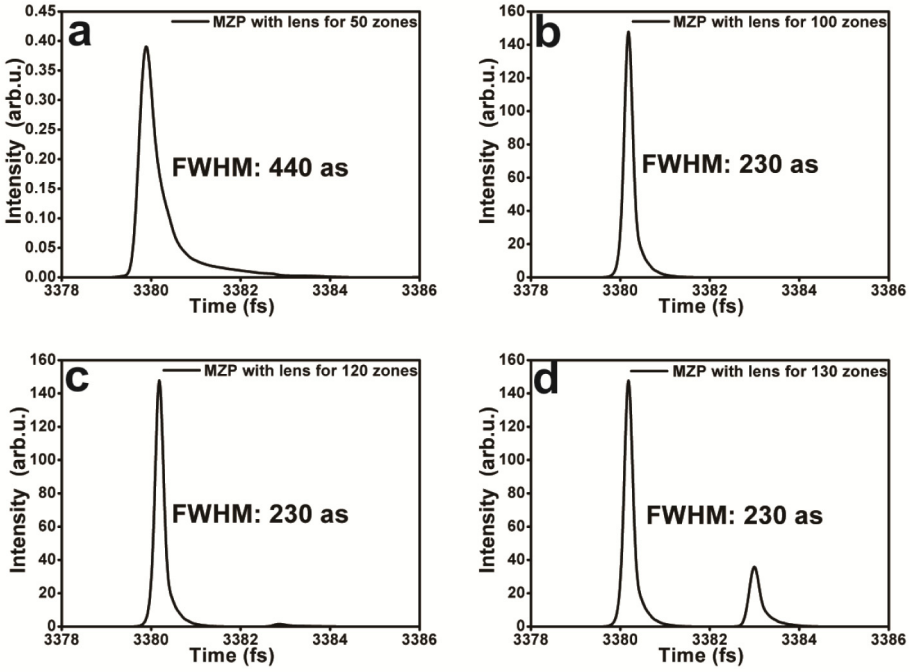

Fig. 7. Temporal intensity distribution of the focused XUV pulse at focus, using the pulse with a duration of 120 as, (a) with 50 zone rings, (b) with 100 zone rings, (c) with 120 zone rings, (d) with 130 zone rings.

4. Conclusion

We have investigated and proven the feasibility of lowering the chromatic dispersion of a Fresnel zone plate under the illumination of broadband attosecond XUV pulses by a special AOD design. Our AOD is a combination of refractive lens and MZP or RZP fabricated on both sides of a 100 nm thick Si_3Ni_4 membrane. Theoretical results show that the time-averaged intensity distribution of lower chromatic dispersion along the optical axis of AODs can be achieved with XUV pulses of 120 as and 500 as. The time-averaged intensity distribution off-axis on the focal plane also shows that the spatial resolution can be improved from 126 nm for the FZP down to 116 nm for the AODs in case of a 120 as XUV pulse, and down to 118 nm for the AODs in case of a 500 as XUV pulse, respectively. Besides the lower chromatic dispersion and higher spatial resolution, AODs can also conserve the temporal pulse structure of 230 as and 535 as at focus, for both 120 as and 500 as pulses, respectively. This AOD design promises a great potential and practical application in time-resolved photoemission XUV microscopy and scanning transmission XUV microscopy, e.g., time-resolved photoemission XUV microscopy in realizing high spatial resolution of 116 nm, while preserving the temporal pulse structure from few hundreds of attoseconds to few femtoseconds.

Acknowledgement

This work was financially supported by the DFG via the Excellence Cluster “Munich-Centre for Advanced Photonics” (MAP, EXC 158) and the MPI-CAS collaboration program.